

A Guide to Molecular Properties from the Bethe–Salpeter Equation

Christof Holzer^{*,†} and Yannick J. Franzke^{*,‡}

[†]*Institute of Theoretical Solid State Physics, Karlsruhe Institute of Technology (KIT),
Wolfgang-Gaede-Straße 1, 76131 Karlsruhe, Germany*

[‡]*Institute of Nanotechnology, Karlsruhe Institute of Technology (KIT), Kaiserstraße 12, 76131
Karlsruhe, Germany*

E-mail: christof.holzer@kit.edu; yannick.franzke@kit.edu

Abstract

The Bethe–Salpeter equation (BSE) combined with the Green’s function *GW* method has successfully transformed into a robust computational tool to describe light-matter interactions and excitation spectra for molecules, solids, and materials from first principles. Thanks to its ability to accurately describe charge-transfer and Rydberg excitations, the *GW*-BSE already forms an established and cost-efficient alternative to time-dependent density functional theory. This raises the question whether the *GW*-BSE approach can become a more general framework for molecular properties beyond excitation energies. In this mini-review, we recapitulate recent endeavors along this point in terms of both theoretical and practical developments for quantum chemistry, physical chemistry, and related fields. In doing so, we provide guidelines for current applications to chemical challenges in collaboration with experimentalists as well as to future developments to extended the *GW*-BSE toolkit.

Introduction

The Bethe–Salpeter equation (BSE) method in the Green’s function *GW* approximation has seen significant success for predicting optical and excitonic spectra in theoretical solid state physics and materials science. In the recent years, the *GW*-BSE also successfully made its transition towards theoretical chemistry,¹ becoming a powerful tool to model light-matter interactions of various molecular systems. Traditionally, these interactions are studied with time-dependent density functional theory (TD-DFT). Here, a linear response equation consisting of the Kohn–Sham orbital eigenvalues and the electronic Hessian, including the two-electron Coulomb and exact exchange interaction as well as the exchange-correlation (XC) kernel, is solved to describe the excited states.² This framework was applied with great success over a wide range of molecular systems, however, the accuracy strongly depends on the chosen functional approximation. Compared to ground-state DFT calculations, it is generally more difficult to find the “right” functional for TD-DFT, as different types of excitations such as charge-transfer (CT), Rydberg, spin-flip, or two-photon excitations may require different functional approximations.

The theoretical foundation of the BSE approach is completely different than that of DFT or TD-DFT, as it is not based on the electron density but on the one-particle Green’s function in a many-body perturbation theory. However, the working equations can be cast into a very similar form. The Kohn–Sham eigenvalues are replaced with the so-called quasiparticle energies from the *GW* method³ and the electronic Hessian does not depend on the XC kernel but the BSE kernel which effectively screens the Coulomb interaction for a given frequency.¹ Therefore, the computational protocol and the costs are similar if suitable approximations such as a static screening are applied to compute the BSE kernel. Then, the only new step in the workflow is the evaluation of the *GW* quasiparticle energies.

The *GW*-BSE has become a major competitor of TD-DFT, with even the static screened kernel outperforming TD-DFT on many occasions at the same computational cost, especially when targeting charge-transfer or Rydberg excitations.^{4–6} As charge-transfer processes are rather common in extended systems, the added reliability of optical excitations obtained from the BSE is highly

valued among researchers. Unlike for DFT and TD-DFT, which have seen 30 years of research being dedicated towards accurately predicting various other properties like non-linear optical properties, direct assessment of excited-state properties and geometries, or even properties unrelated to optical spectra as, for example, nuclear magnetic resonance (NMR) properties, the applicability of the BSE to these properties is still rather narrow. This review will therefore focus on this extended set of molecular properties, and outline the development and application of advanced algorithms enabling the BSE to be applied to a more diverse set of common tasks in computational spectroscopy. An overview of molecular property operators that have already been assessed within the framework of the BSE is given in Table 1.

In the subsequent sections, we will refer to operators generally as \hat{v} , with Table 1 providing the appropriate notation. Molecular properties are subsequently obtained from these operators in a linear or on-linear response framework. This allows to transfer many algorithmic developments for TD-DFT to the BSE framework, transforming it into a full-fledged computational tool for chemistry, physics, and materials science.

Table 1: Common property operators for which the BSE has already been applied. α is the Sommerfeld fine structure constant, c the speed of light, \vec{r} the position vector, \vec{B} the magnetic field, and \vec{p} the momentum operator. \vec{s} denotes the spin of an electron, and Z_K the charge of the K -th nucleus. SOMF refers to the spin-orbit mean field approach.

| Name | Symbol | Operator \hat{v} |
|----------------------------|---------------------|---|
| electric dipole (length) | μ | \vec{r} |
| electric dipole (velocity) | p | $-i\vec{\nabla}$ |
| magnetic dipole | m | $\vec{r} \times \vec{B}$ |
| Fermi contact | h_K^{FC} | $(8\pi\alpha^2/3) \delta(\vec{r}_K)\vec{s}$ |
| spin-dipole | h_K^{SD} | $\alpha^2 (3\vec{r}_K^\dagger \vec{s} \vec{r}_K - r_K^2 \vec{s}) / r_K^5$ |
| paramagnetic spin-orbit | h_K^{PSO} | $-i\alpha^2 (\vec{r}_K \times \vec{\nabla}) / r_K^3$ |
| one-electron SOMF | h_1^{SOMF} | $\sum_K Z_K (\vec{r}_K \times \vec{p}) / 2c^2 r_K^3$ |
| two-electron SOMF | h_2^{SOMF} | $(\vec{r} \times \vec{p}) / 2c^2 r^3$ |

Excited States from the BSE

Before explicitly discussing molecular properties, we first need to have a short look at the underlying poles of the linear response problems, with the latter also resembling the excited states. Within the *GW*-BSE method, excited states can be extracted from the general eigenvalue problem⁶⁻⁹

$$\begin{pmatrix} \mathbf{A}(\Omega) & \mathbf{B}(\Omega) \\ \mathbf{B}^*(\Omega) & \mathbf{A}^*(\Omega) \end{pmatrix} \begin{pmatrix} X \\ Y \end{pmatrix} = \Omega \begin{pmatrix} \mathbf{1} & \mathbf{0} \\ \mathbf{0} & -\mathbf{1} \end{pmatrix} \begin{pmatrix} X \\ Y \end{pmatrix} \quad (1)$$

with the electronic Hessian consisting of the the matrices \mathbf{A} and \mathbf{B} being defined as¹⁰

$$A_{ai,bj} = (\varepsilon_a - \varepsilon_i) \delta_{ab} \delta_{ij} + (ai|jb) - (ab|ji) - \Xi_{ab,ji}(\Omega) \quad (2)$$

$$B_{ai,bj} = (ai|bj) - (aj|bi) - \Xi_{bi,aj}(\Omega) \quad (3)$$

and the solution vectors $\{\mathbf{XY}\}$ being normalized to the condition

$$X_N X_M^\dagger - Y_N Y_M^\dagger = \delta_{NM} \quad (4)$$

where N and M denote different solutions or excited states. ε_i and ε_a are the *GW* quasiparticles of the occupied (i, j, \dots) and the virtual states (a, b, \dots). These may be calculated with the one-shot G_0W_0 , the iterative eigenvalue-only self-consistent *evGW*, or the full quasiparticle self-consistent *qsGW* approximation.¹¹ The frequency-dependent BSE kernel $\Xi(\Omega)$ is given as

$$\Xi_{pq,rs}(\Omega) = \frac{i}{2\pi} \int d\omega' e^{-i\Omega\omega'^+} W_{pq,rs}(\Omega) \left[\frac{1}{\Omega - \omega' - (\varepsilon_q - \varepsilon_r) + i\eta} + \frac{1}{\Omega + \omega' - (\varepsilon_p - \varepsilon_s) + i\eta} \right] \quad (5)$$

where p, q, r, s denote general states. Here, the screened Coulomb interaction \mathbf{W} is defined as

$$W_{pq,rs}(\Omega) = \sum_{tu} \kappa_{pq,tu}^{-1}(\Omega) (tu|rs) \quad (6)$$

with the dielectric function κ . The screened Coulomb interaction is commonly used also in the preceding GW step within a GW -BSE implementation. Efficient procedures to evaluate Eq. 6 for arbitrary values of Ω have been outlined in literature, and especially $\Omega = 0$ can be evaluated very efficiently as it is always Hermitian positive definite.^{9,12} We note that the first common approximation has already been applied to Eqs. 1 to 5. To arrive at this result, the BSE kernel is approximated as¹

$$if^{\text{BSE}} = \mathbf{v} + \frac{\partial \Sigma}{\partial \mathbf{G}} \xrightarrow{\text{GWA}} \mathbf{v} + \frac{\partial \mathbf{GW}}{\partial \mathbf{G}} \xrightarrow{\frac{\partial W}{\partial G}=0} \mathbf{v} - \mathbf{\Xi}(\Omega) \quad (7)$$

subsequently applying the GW approximation (GWA) to the self-energy Σ neglecting the partial derivative resulting from the screened Coulomb interaction \mathbf{W} being also implicitly dependent on the Green's function \mathbf{G} . In Eq. 7, \mathbf{v} denotes the bare Coulomb interaction, giving rise to an exchange term. Solving the frequency dependent Eq. 1 is still rather involved, with the calculation of Eq. 5 being the time-limiting step. Therefore, usually another approximation is invoked,

$$\mathbf{\Xi}(\Omega) \approx \mathbf{W}(\Omega = 0) \quad (8)$$

This leads to the the static screened approximation of the BSE, reducing the computational demands by one to two orders of magnitude if approximations such as the resolution-of-the-identity (RI) approximation¹³ are used. Compared to the fully dynamic BSE method, errors of 0.1 to 0.3 eV are observed,¹⁴ outlining that the applied approximations are not entirely harmless, but more of a necessity to make the BSE competitive with time-dependent density functional theory. Further analyzing the matrix elements of Eq. 2 and 3 in more detail, Rohlfing and Louie noted that the direct part of the electron-hole interaction kernel involving \mathbf{W} mainly controls the interactions between the quasihole and quasiparticle states, while the exchange parts with \mathbf{v} tune the splitting between singlet and triplet excitations.¹⁴ In the last few years, a notable deficiency of the static screened BSE approximation to describe triplet states has been noted, and indeed this can be traced back to an overscreening from the bare Hartree–Fock (HF) exchange term, arising from neglecting higher-order derivatives of the screened exchange. Even given this partly severe drawbacks, the static

screened BSE has become the de-facto standard in current applications of the *GW*-BSE method in both theoretical chemistry and solid state physics, which can mostly be attributed to the superior numerical scaling of its implementations. Current implementation manage to predict optical spectra sizable systems composed of well over 100 atoms.^{1,12,15-17}

Simplifications for Real-Valued Orbitals

Similar to TD-DFT, for real-valued molecular orbitals, the generalized BSE eigenvalue problems can be converted into a set of two symplectic eigenvalue problems. This allows for a more concise calculation of properties in many cases. The two coupled symplectic eigenvalue problems read

$$[(\mathbf{A} - \mathbf{B})(\mathbf{A} + \mathbf{B})](X + Y) = \Omega^2(X + Y) \quad (9)$$

$$[(\mathbf{A} + \mathbf{B})(\mathbf{A} - \mathbf{B})](X - Y) = \Omega^2(X - Y) \quad (10)$$

with the matrices $(\mathbf{A} + \mathbf{B})$ and $(\mathbf{A} - \mathbf{B})$ simply defined as linear combinations of the previously outlined matrices \mathbf{A} and \mathbf{B}

$$(A + B)_{ai,bj} = (\epsilon_a - \epsilon_i)\delta_{ab}\delta_{ij} + H_{ai,bj}^+(\Omega) \quad (11)$$

$$(A - B)_{ai,bj} = (\epsilon_a - \epsilon_i)\delta_{ab}\delta_{ij} + H_{ai,bj}^-(\Omega) \quad (12)$$

Within Eqs. 9 and 10, both the right $(X + Y)$ and left $(X - Y)$ solutions are normalized to obey the relation

$$\langle (X + Y)_N | (X - Y)_M \rangle = \delta_{NM} \quad (13)$$

The linear combinations of the Coulomb, unscreened exchange, and screened Coulomb terms read

$$H_{pq,rs}^{+,BSE}(\Omega) = (pq|rs) - (ps|rq) - (pr|sq) - \Xi_{ps,rq}(\Omega) - \Xi_{pr,sq}(\Omega) \quad (14)$$

$$H_{pq,rs}^{-,BSE}(\Omega) = (ps|rq) - (pr|sq) + \Xi_{ps,rq}(\Omega) - \Xi_{pr,sq}(\Omega) \quad (15)$$

These linear combinations provide the significant advantage of being either symmetric (+) or skew-symmetric (−) with respect to interchanges in indices. They can therefore be directly related to properties with symmetric (real) operators, as for example electric fields, or to properties with skew-symmetric (imaginary) operators, as for example magnetic fields. While rewriting the eigenvalue problem is also possible for complex molecular orbitals, this symmetry correspondence is lost. Therefore, in the case of complex orbitals, the advantages of using Eqs. 9 and 10 over Eq. 1 are limited.¹⁸ Complex orbitals are needed for, e.g., calculations in finite magnetic fields or relativistic approaches treating spin–orbit coupling variationally in the ground state.

Optical Linear Response Properties

In linear response theory, the corresponding linear response function of a system with respect to a time-dependent field oscillating with the frequency ω can be written as^{19,20}

$$\langle\langle v^\zeta; v^\eta(\omega) \rangle\rangle = \text{Tr}(\hat{v}^\zeta \gamma^\eta(\omega)) \quad (16)$$

with the property operator \hat{v}^ζ describing the perturbation ζ and the first-order reduced density matrix γ^η of the perturbation η ,

$$\gamma^\eta = \begin{pmatrix} 0 & X^\eta \\ Y^\eta & 0 \end{pmatrix} \quad (17)$$

Using these definitions, determining linear optical response properties from the BSE is straightforward, as one simply needs to modify the general eigenvalue problem to instead determine the components of the frequency-dependent first-order transition density matrices. Assuming that the general property vectors P and Q collect the integrals of the external perturbation,

$$\langle \phi_a | \hat{v}^\eta | \phi_i \rangle = P_{ai} = Q_{ia}^* \quad (18)$$

the coupled-perturbed BSE equations reads

$$\left[\begin{pmatrix} \mathbf{A}(\omega) & \mathbf{B}(\omega) \\ \mathbf{B}^*(\omega) & \mathbf{A}^*(\omega) \end{pmatrix} - \omega \begin{pmatrix} \mathbf{1} & \mathbf{0} \\ \mathbf{0} & -\mathbf{1} \end{pmatrix} \right] \begin{pmatrix} X \\ Y \end{pmatrix} = \begin{pmatrix} P \\ Q \end{pmatrix} \quad (19)$$

The right-hand side (RHS) of Eq. 19 is solely determined by the external perturbation, e.g. an electric field oscillating with the frequency ω and not by the excited states Ω . In Ref. 21, it was therefore outlined that in cases where many excited states exist in or before the energetic region of interest, Eq. 19 can be used to efficiently bypass the overhead of calculating many excited states from the BSE eigenvalue problem. To obtain an optical spectrum, consequently the frequency-dependent dipole polarizability is calculated directly from the solutions of Eq. 19 via a direct product,

$$\alpha^{\eta\zeta}(\omega) = \langle P^\eta, Q^\eta | X^\zeta(\omega), Y^\zeta(\omega) \rangle \quad (20)$$

Within the full frequency-dependent BSE, this is even simpler than the general eigenvalue problem: Unlike the energies of the excited states Ω , the frequency of the external field ω is already known *a priori*! Therefore, the left-hand side (LHS) of the coupled-perturbed equation 19 does not change during an iterative procedure. If real orbitals are used as outlined in the previous section, the coupled-perturbed linear response equation can be rewritten as

$$[(\mathbf{A}(\omega) + \mathbf{B}(\omega))(X + Y) - \omega(X - Y)] = -(P + Q) \quad (21)$$

$$[(\mathbf{A}(\omega) - \mathbf{B}(\omega))(X - Y) - \omega(X + Y)] = -(P - Q) \quad (22)$$

From Eqs. 18, 21, and 22 it can be concluded that $(P + Q)$ is zero for purely imaginary operators, while $(P - Q)$ is zero for purely real operators. Note that for any non-vanishing frequency ω , both equations are strictly coupled and neither part can be neglected. Still, instead of one eigenvalue problem of full size, two with half the original size can be solved. Caution must, however, be used, as in the limiting case of the frequency of the external perturbation approaching an excited state, $\omega \rightarrow \Omega$, the coupled-perturbed Bethe–Salpeter equations will diverge. It is therefore often neces-

sary to assume that the external perturbation has a constant imaginary component, $\omega = \omega_r + \Gamma$, “damping” the diverging cases. The assumed imaginary component directly leads to a broadening of the polarizability spectra with a Lorentzian line shape.

The ability to bypass lower-lying states can for example be utilized to assess core excited states without neglecting or projecting out valence orbitals, as shown in Figure 1. Given the high performance of the *GW*-BSE method for core excited states,²² this is a significant progress in the prediction of K- or L-edges. Figure 1 further outlines that indeed common approximations used, such as the core-valence separation (CVS) approximation, are usually well suited for the extraction of core excited states, though the implementation of complex dynamic polarizabilities allows for a convenient yet efficient way of checking this approximation if there is doubt about its reliability.

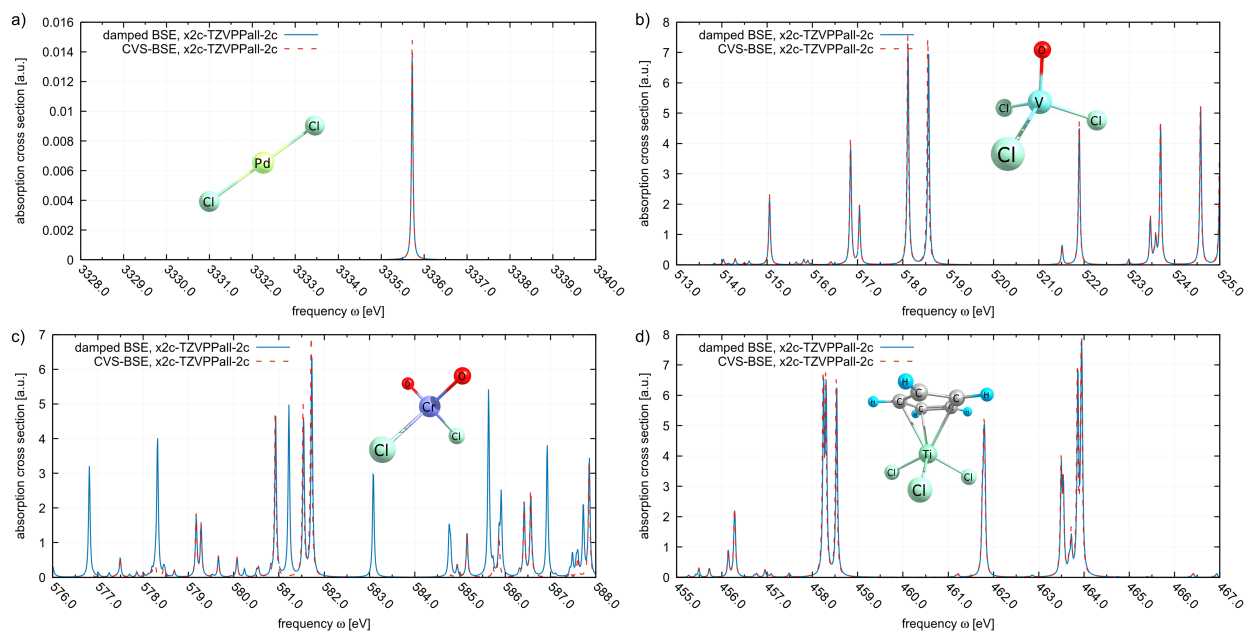


Figure 1: Damped response BSE (blue solid lines) and CVS-BSE XAS spectra (red dashed lines) comparing the energy-integrated absorption cross section of a) the PdCl₂ L₂-edge, b) the VOCl₃ L_{2,3}-edges, c) the CrO₂Cl₂ L_{2,3}-edges, and d) the TiCpCl₃ L_{2,3}-edges. All spectra calculated at the frequency-sampled contour deformation $G_0W_0@TMHF$ level of theory. A damping parameter of 0.02 eV was used for damped response BSE. CVS-BSE spectra were broadened accordingly with Lorentzians. Absorption cross section given in atomic units (= Hartree · bohrs²), frequency in eV. Scalar-relativistic and spin-orbit effects are introduced with exact two-component (X2C) theory. Reprinted from M. Kehry, W. Klopper, C. Holzer, *J. Chem. Phys.* **2023**, 159, 044116. Copyright the Authors. Licensed under a Creative Commons Attribution (CC BY) license (<https://creativecommons.org/licenses/by/4.0/>).

The equations outlined in this section can generally be used to calculate linear response properties of molecular systems, as long as one can formulate the appropriate RHS in terms of integrals also expressible in the same basis of molecular orbitals. This encompasses, for example, static and dynamic polarizabilities, optical rotation tensors, or dynamic magnetizabilities. To illustrate this point, results for static dipole polarizabilities of the metallocenes FeCp₂, RuCp₂, and OsCp₂ are presented in Table 2. Here, the electric dipole operator represents the perturbations ζ and η . The Kohn–Sham DFT approach underestimates the polarizabilities of all three complexes and the *GW*-BSE reduces the deviation towards the experiment.²³ *GW*-BSE@PBE is able to recapture the experimental trend of a monotonous increase of the polarizability with increasing mass for these metallocenes. The good performance of *GW*-BSE is not restricted to static polarizabilities but also dynamic polarizabilities are obtained in good agreement with the experiment.^{21,24}

Table 2: Static polarizabilities for group 8 metallocenes in atomic units at the Kohn–Sham DFT and *GW*-BSE levels with the dhf-TZVP basis set. Computational results are taken from Ref. 21 and compared to the experimental findings (Expt.) of Ref. 23.

| | CAM-B3LYP | | PBE0 | | Expt. |
|-------------------|-----------|----------------|-------|----------------|-------|
| | DFT | <i>GW</i> -BSE | DFT | <i>GW</i> -BSE | |
| FeCp ₂ | 118.3 | 128.3 | 118.8 | 131.3 | 126.1 |
| RuCp ₂ | 127.6 | 132.0 | 128.1 | 134.2 | 133.1 |
| OsCp ₂ | 128.0 | 130.6 | 128.7 | 137.9 | 138.5 |

Optical Non-Linear Response Properties

Non-linear optical properties are more tedious to obtain. For example, for non-linear hyperpolarizabilities, multiple external fields with different frequencies ω act on the system, leading to a distinctly more involved response of the latter. Accordingly, the second-order reduced density matrix^{25,26}

$$\gamma^{\zeta\eta} = \begin{pmatrix} K^{\zeta\eta} & X^{\zeta\eta} \\ Y^{\zeta\eta} & K^{\zeta\eta} \end{pmatrix} \quad (23)$$

is needed to evaluate the quadratic response functions

$$\langle\langle v^\zeta; v^\eta(\omega), v^\theta(\omega') \rangle\rangle = \text{Tr}\left(\hat{v}^\zeta \gamma^{\eta\theta}(\omega, \omega')\right) \quad (24)$$

Note that the response is assumed to be instantaneous and independent, so that the order in which the frequency-dependent external perturbations $v^\eta(\omega)$ and $v^\theta(\omega')$ are applied does not matter. The diagonal matrix elements \mathbf{K} can be obtained directly from the linear response functions,

$$K_{ij}^{\zeta\eta} = -\sum_a \left[X_{aj}^\zeta Y_{ai}^\eta + Y_{ai}^\zeta X_{aj}^\eta \right] \quad (25)$$

$$K_{ab}^{\zeta\eta} = \sum_i \left[Y_{bi}^\zeta X_{ai}^\eta + X_{ai}^\zeta Y_{bi}^\eta \right] \quad (26)$$

Contrary, the off-diagonal matrix elements $X^{\zeta\eta}$ and $Y^{\zeta\eta}$ need to be determined from another linear problem of the same structure as Eq. 19, with $\omega = \omega^\zeta + \omega^\eta$ and P and Q replaced by their quadratic response analogues²⁶

$$P_{ai}^{\zeta\eta} = \sum_b \left(U_{ab}^\zeta X_{bi}^\eta + U_{ab}^\eta X_{bi}^\zeta \right) - \sum_j \left(U_{ij}^\zeta X_{aj}^\eta + U_{ij}^\eta X_{aj}^\zeta \right) + g_{ai}^{\text{BSE}}(X^\zeta, Y^\zeta; X^\eta, Y^\eta) \quad (27)$$

$$Q_{ai}^{\zeta\eta} = \sum_b \left(V_{ab}^\zeta Y_{bi}^\eta + V_{ab}^\eta Y_{bi}^\zeta \right) - \sum_j \left(V_{ij}^\zeta Y_{aj}^\eta + V_{ij}^\eta Y_{aj}^\zeta \right) + g_{ia}^{\text{BSE}}(X^\zeta, Y^\zeta; X^\eta, Y^\eta) \quad (28)$$

with

$$U_{pq}^\zeta = \sum_{bj} A'_{pq,bj} X_{bj}^\zeta + B_{pq,bj} Y_{bj}^\zeta + v_{pq}^\zeta \quad (29)$$

$$V_{pq}^\zeta = \sum_{bj} B_{pq,bj}^* X_{bj}^\zeta + A'_{pq,bj}^* Y_{bj}^\zeta + v_{pq}^{\zeta,*} \quad (30)$$

The matrix \mathbf{A}' denotes a slightly modified Eq. 2, where the quasiparticle energy differences have been dropped:

$$A'_{pq,rs} = (pq|sr) - (pr|sq) - \Xi_{pr,sq}(\Omega) \quad (31)$$

Upon inspection of Eqs. 25 to 28, the symmetry upon switching the perturbations ζ and η is obvious, again outlining that the order of applying the perturbations does not matter for anything other than indexing purposes. We remind the reader that again simplifications can be made for purely real orbitals, though it is not necessary to repeat those, as a detailed outline of the corresponding formulas has been given in Ref. 26. Another key approximation has been made in the determination of Eqs. 27 and 28 by again neglecting hyperkernel derivatives. Following the approximations made for the BSE kernel, which explicitly neglect the derivative of the screened Coulomb part with respect to the Greens function leads to^{27,28}

$$g^{\text{BSE}} = \frac{\partial^2 \Sigma}{\partial \mathbf{G} \partial \mathbf{G}} \xrightarrow{\text{Eq.7}} \frac{\partial \mathbf{W}}{\partial \mathbf{G}} \xrightarrow{\frac{\partial W}{\partial G} = 0} 0 \quad (32)$$

The BSE hyperkernel g^{BSE} is therefore set to zero, though the impact of this approximation has not yet been assessed in detail.

Table 3 illustrates the application of the *GW*-BSE to the hyperpolarizabilities of small molecules. Conventional DFT methods such as CAM-B3LYP and PBE0 lead to a significant deviation from the experiment. *GW*-BSE substantially improves the results and leads to an excellent agreement with the experimental findings when using well suited Kohn–Sham starting points such as the TMHF functional, which was also successfully applied in the previous section for linear response properties. That is, the behavior in terms of the Kohn–Sham reference is well transferred to higher-order derivatives, suggesting that a single reference can be used for a wide range of optical properties in the *GW*-BSE. Based on the given results, neglecting the BSE hyperkernel also seems to be well justified for hyperpolarizabilities.

Besides the hyperkernel, two-photon absorption processes can also be described within a non-linear regime. Therefore, the *GW*-BSE is now able to account for all common sorts of excitations.

Table 3: Dynamic first hyperpolarizability $\beta_{||}$ (in atomic units) for H₂O, MeOH (Me = CH₃), and dimethyl ether (DME) at 1064 nm calculated at the Kohn–Sham DFT and *GW*-BSE levels with the d-aug-cc-pVQZ basis set. Computational results are taken from Ref. 26 and compared to the experimental findings (Expt.) of Refs. 29 (H₂O, MeOH) and 30 (DME).

| Method | H ₂ O | MeOH | DME |
|---|------------------|-------------|--------------|
| CAM-B3LYP | −17.7 | −35.0 | −102.9 |
| PBE0 | −19.5 | −40.7 | −119.3 |
| <i>G</i> ₀ <i>W</i> ₀ -BSE@PBE0 | −20.6 | −42.8 | −126.3 |
| ev <i>GW</i> -BSE@PBE0 | −18.2 | −38.7 | −111.5 |
| <i>G</i> ₀ <i>W</i> ₀ -BSE@TMHF | −18.6 | −34.8 | −105.0 |
| ev <i>GW</i> -BSE@TMHF | −16.7 | −32.5 | −96.4 |
| Expt. | −19.2 ± 0.9 | −31.2 ± 1.6 | −94.0 ± 0.25 |

Transition Moments Between Excited States

Again similar to TD-DFT, also properties between excited states are of growing interest, leading to the possibility to predict, for example, transient absorption. Intrinsically, calculating a property that involves an expectation value between two excited states is very similar to calculating non-linear properties as outlined in the previous section. The second-order reduced density matrix only needs to be slightly modified, yielding²⁸

$$\boldsymbol{\gamma}^{NM} = \begin{pmatrix} \mathbf{K}^{NM} & \mathbf{X}^{NM} \\ \mathbf{Y}^{NM} & \mathbf{K}^{NM} \end{pmatrix} \quad (33)$$

From the second-order response matrix, the corresponding transition property between two excited states *N* and *M* can be calculated similar to Eq. 24, by choosing to let the frequency of the perturbation approach the energy of the excited states,

$$v_{NM} = \lim_{\omega \rightarrow \Omega_N} (\omega - \Omega_N) \lim_{\omega' \rightarrow -\Omega_M} (\omega' + \Omega_M) \times \langle\langle v^\zeta; v^\eta(\omega), v^\theta(\omega') \rangle\rangle = \text{Tr} \left(\hat{v}^\zeta \boldsymbol{\gamma}^{NM} \right) \quad (34)$$

Note that in Eq. 34 the selection of excited states matter, and generally $\boldsymbol{\gamma}_{NM} \neq \boldsymbol{\gamma}_{MN}$. The matrix elements of $\boldsymbol{\gamma}_{NM}$ can be evaluated similar to the previous section with the matrix elements of \mathbf{K}

being defined as

$$K_{ij}^{NM} = - \sum_a [X_{ja}^N X_{ai}^{*M} + Y_{ai}^N Y_{aj}^{*M}] \quad (35)$$

$$K_{ab}^{NM} = \sum_i [X_{bi}^N X_{ai}^{*M} + Y_{ai}^N Y_{bi}^{*M}] \quad (36)$$

The corresponding RHS needed to evaluate Eq. 19 is then obtained as

$$P_{ai}^{NM} = \sum_b (U_{ab}^N X_{bi}^{*M} + U_{ab}^M Y_{bi}^N) - \sum_j (U_{ij}^N X_{aj}^{*M} + U_{ij}^M Y_{aj}^N) \quad (37)$$

$$Q_{ai}^{NM} = \sum_b (V_{ab}^N Y_{bi}^{*M} + V_{ab}^M X_{bi}^N) - \sum_j (V_{ij}^N Y_{aj}^{*M} + V_{ij}^M X_{aj}^N) \quad (38)$$

with

$$U_{pq}^N = \sum_{bj} A'_{pq,bj} X_{bj}^N + B_{pq,bj} Y_{bj}^N \quad (39)$$

$$V_{pq}^N = \sum_{bj} B^*_{pq,bj} X_{bj}^N + A'^*_{pq,bj} Y_{bj}^N \quad (40)$$

The hyperkernel contribution has again been dropped. The frequency of at which Eq. 19 needs to be evaluated with the constructed RHS is exactly $\omega = \Omega_M - \Omega_N$. If the excited states N and M are switched in Eq. 34, instead of the eigenpair $\omega, \{\mathbf{X}, \mathbf{Y}\}$, the time-reversal symmetry related eigenpair $-\omega, \{\mathbf{Y}^*, \mathbf{X}^*\}$ is to be used. As a consequence, upon the interchange $N \leftrightarrow M$, also $\mathbf{X} \rightarrow \mathbf{Y}^\dagger$ and $\mathbf{Y} \rightarrow \mathbf{X}^\dagger$ must be interchanged accordingly in the second-order reduced density matrix. Evaluating the matrices \mathbf{K} with interchanged indices also leads to the corresponding adjoint matrix, resulting in the relation $\boldsymbol{\gamma}_{NM} = (\boldsymbol{\gamma}_{MN})^\dagger$. Transition properties originating from purely real operators are therefore unaffected by interchanging excited states N and M , while purely imaginary transition properties switch signs.

Calculating transition moments between excited states is of high interest in the field of optical materials, as for example, in the design of organic light emitting diodes (OLEDs). The prototype complex tris-bipyridin ruthenium $[\text{Ru}(\text{bpy})_3]^{2+}$ acts via an intersystem crossing (ISC) mechanism

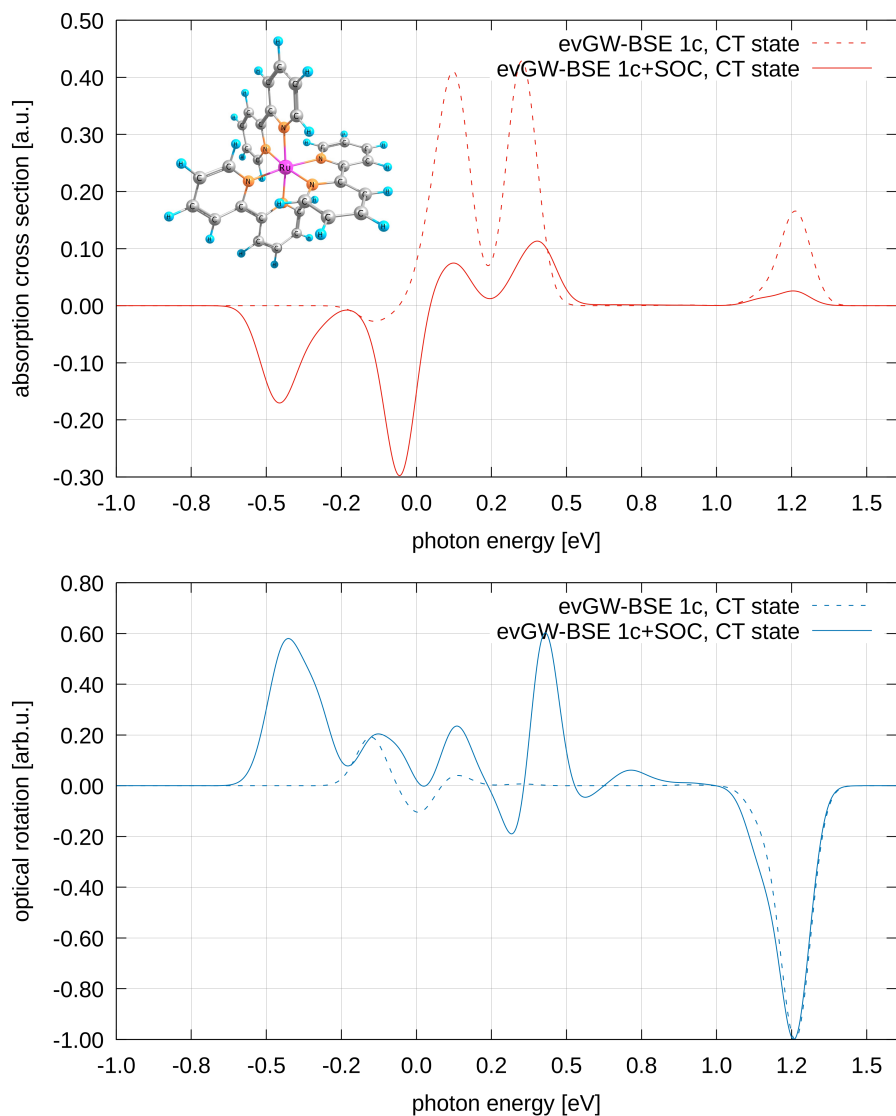


Figure 2: Predicted *evGW*-BSE transient absorption (upper) and optical rotation (lower) spectra of $[\text{Ru}(\text{bpy})_3]^{2+}$ obtained from scalar-relativistic (1c, dotted line) and scalar-relativistic plus perturbative spin-orbit coupling (1c+SOC, solid line). Negative oscillator strengths correspond to emission lines. An arbitrary broadening of 0.05 eV is applied. The absorption cross section at 0.0 eV is an artifact of this broadening. Absorption cross section given in atomic units (a.u.), optical rotation in arbitrary units (arb.u.). Reprinted (adapted) from P. Himmelsbach, C. Holzer, *J. Chem. Phys.* **2024**, *161*, 241105. Copyright the Authors. Licensed under a Creative Commons Attribution NonCommercial 4.0 International (CC BY-NC) license (<https://creativecommons.org/licenses/by-nc/4.0/>).

starting from an excited ligand-to-metal charge transfer (LMCT) state, which is hard to capture correctly with TD-DFT unless careful functional tuning and testing is carried out. *GW*-BSE on the other hand can perfectly reproduce these LMCT states, and also yield sufficient predictive power

for excited-state transitions, even including ISC when spin-orbit coupling is included. Figure 2 outlines the transient absorption spectra simulated using *evGW*-BSE, with and without including spin-orbit coupling (SOC). Clearly, including spin-orbit coupling is instrumental in finding the correct S→T transition. Having a method at hand that is able to describe both LMCT transitions and SOC effects is highly valuable for researching advanced materials for light-matter interactions, and the *GW*-BSE method is currently progressing to the forefront of this branch of research.

Excited-State Dipole Moments and an Outlook on Gradients

Recently, Ref. 27 has devised a way to also calculate excited-state dipole moments, which are conceptually very close also to analytic excited state gradients. The excited-state dipole moments can be assessed in an indirect way, calculating the difference of the excited-state dipole moment and ground-state dipole moment,

$$\mu_{\alpha}^N - \mu_{\alpha}^0 = \frac{\partial \Omega^N}{\partial E_{\alpha}} \quad (41)$$

with the Cartesian component α and the excited state N . The difference dipole moment can be determined from the derivative of the excited-state energy with respect to an electric field E_{α} . While Villalobos-Castro *et al.* have used a Lagrangian Z-vector formalism in Ref. 27 to arrive at an explicit formulation, the coupled-perturbed approach outlined for non-linear properties can also be used. Assuming that the transition of interest is the $N \leftrightarrow N$ transition, the excited-state dipole moment is obtained as

$$\mu_{\alpha}^N = \text{tr}(\hat{\mu}_{\alpha} \bar{\gamma}^{NN}) \quad (42)$$

Following Ref. 27, the corresponding coupled-perturbed equation that needs to be solved is similar to those needed to be solved for excited-state properties. $\bar{\gamma}^{NN}$ differs from γ^{NN} just by the modification of the RHS in Eqs. 37 and 38, now including the contribution of the ground-state

Hamiltonian, yielding

$$P_{ai}^{NM} = \sum_b (U_{ab}^N X_{bi}^{*M} + U_{ab}^M Y_{bi}^N) - \sum_j (U_{ij}^N X_{aj}^{*M} + U_{ij}^M Y_{aj}^N) + \sum_{bj} H_{ai,bj}^{\text{KS}} K_{bj} \quad (43)$$

$$Q_{ai}^{NM} = \sum_b (V_{ab}^N Y_{bi}^{*M} + V_{ab}^M X_{bi}^N) - \sum_j (V_{ij}^N Y_{aj}^{*M} + V_{ij}^M X_{aj}^N) + \sum_{bj} H_{ai,bj}^{\text{KS}} K_{bj} \quad (44)$$

Contributions from the quasiparticle *GW* step to the RHS have been neglected.²⁷ \mathbf{H}^{KS} denotes the Kohn–Sham kernel of the underlying density functional approximation.³¹ The resulting solution vector $\{\mathbf{X}, \mathbf{Y}\}$ is often referred to as Z-vector in gradient calculations, and can be used to determine both excited-state dipole moments as well as analytic gradients, though for the latter some more ingredients are needed.²⁷ At the time of writing, the Z-vector equations have only seen exploratory use to determine excited-state dipole moments with great success.^{32,33} This is illustrated for the excess dipole moment (S_1 excited state) of push-pull oligomers in Figure 3. The comparison between the finite-field (ff) calculations and the Z-vector (Z) approach outlines that the latter leads to the qualitatively correct behavior, however, setting the screened Coulomb potential to its zero-field value and approximating the *evGW* quasiparticle energies with the Kohn–Sham values leads to notable deviations. Compared to the underlying Kohn–Sham methods, which diverges, this Z-vector ansatz still leads to a tremendous improvement, as the correct behavior of the excess dipole moment having a maximum at a certain chain length is recovered. PBE0 fails to recover this trend completely, leading to unphysical increases of the excess dipole moment with increased chain length. This divergence is due to the too small amount of exact exchange in the long-range region and could be removed with range-separated or optimally tuned functionals. However, the *GW*-BSE naturally resolves all issues in a more rigorous way from first principles.

The explicit usefulness of gradients remains to be shown, but initial investigations point at BSE gradients being very useful,^{34,35} though the necessary *GW* contribution to the gradient remains problematic to date.²⁷

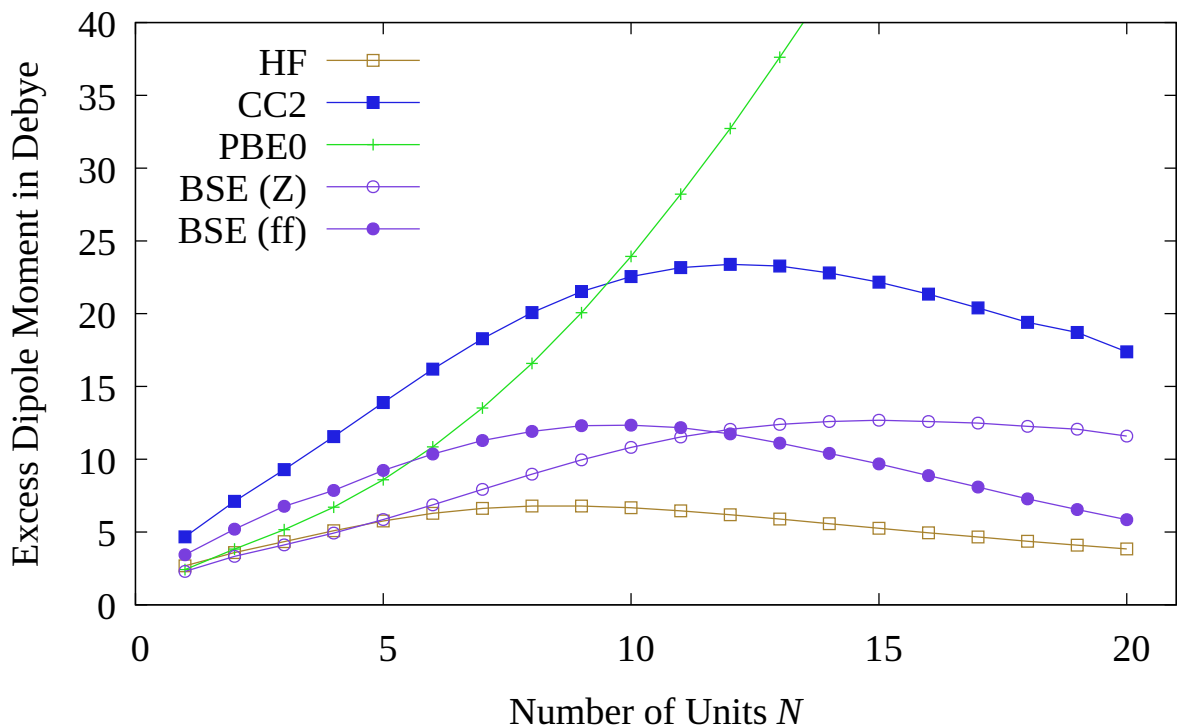


Figure 3: Excess dipole moment of the S_1 excited state of the push-pull oligomers $H_2N - [CH = CH]_N - NO_2$ for various system sizes. Calculations are performed at the time-dependent HF, linear-response CC2 (relaxed), PBE0 TDDFT, and the *evGW*-BSE@PBE0 levels using the cc-pVTZ basis set. BSE results are shown for the finite-field (ff) approach using a 5-point stencil formula and the analytical Z-vector (Z) approach. The excess dipole moment is defined as the norm of the vector difference in Eq. 41. Individual data for plot taken from Refs. 27 (BSE Z-vector) and 33 (other methods).

NMR Spin–Spin Coupling Constants

So far, this mini-review exclusively presented the application of the *GW*-BSE to optical properties or light-matter interactions. Given the success in this field, applications to other research areas are of interest. NMR spin–spin coupling constants (SSCCs) are closely related to optical excitations in terms of a computer implementation.³⁶ The total SSCC consists of three first-order response terms, namely the Fermi-contact (FC), spin-dipole (SD), and the paramagnetic spin-orbit (PSO) term, as well as the diamagnetic spin-orbit (DSO) interaction, which is directly available from the ground-state density matrix. Usually, the latter is small and the coupling constant is dominated by the response terms. Here, the FC and SD interactions act as a real triplet operator, while the PSO

term is of imaginary singlet character. This allows to apply the *GW*-BSE in a post-Kohn–Sham fashion to improve the DFT performance for these three terms by solving the static linear response equation³⁷

$$\begin{pmatrix} \mathbf{A} & \mathbf{B} \\ \mathbf{B}^* & \mathbf{A}^* \end{pmatrix} \begin{pmatrix} X \\ Y \end{pmatrix} = \begin{pmatrix} P \\ Q \end{pmatrix} \quad (45)$$

where the RHS $P_{ai} = Q_{ia}^*$ denotes the respective perturbation operator (FC, SD, PSO) in the molecular orbital basis, c.f. Eq. 18. The NMR coupling tensor is then obtained by the static form of Eq. 20. Just like the dynamic generalization in Eq. 19, this equation can be simplified again and the perturbations operators can be treated separately for real-valued orbitals, i.e. the FC and SD terms are available from the symmetric linear combination and the PSO interaction is obtained from the skew-symmetric one. This way, the NMR coupling constants are efficiently obtained in a non-relativistic³⁶ or scalar-relativistic framework.³⁸ For complex-valued orbitals, which are obtained in self-consistent relativistic spin–orbit calculations,³⁹ the terms are coupled and Eq. 45 is solved without simplifications.

A first benchmark study was performed in Ref. 37 for a set of organic molecules with CC3 serving as reference and results were compared to Kohn–Sham DFT. Often, the FC interaction is the dominant contribution and the *GW*-BSE does not improve upon DFT. Due to the relation of the FC term to triplet excitations, this property is a serious challenge for *GW*-BSE as illustrated in Figure 4. Generally, benchmark studies have shown that *GW*-BSE performs much better for singlet excitations than triplet excitations.^{4,40,41} Therefore, the correlation-kernel augmented Bethe–Salpeter equation (cBSE) was introduced in Ref. 42, which computes the screened exchange with the Kohn–Sham orbitals and includes the correlation part of the XC kernel in the electronic Hessian of the BSE. This improves the description of triplet excitations, while retaining the correct description of charge-transfer processes. According to Figure 4, cBSE also improves the accuracy of NMR coupling constants. As no qs*GW* is used, the underlying functional has to incorporate a large amount of exact exchange such as in Becke’s half and half functional (BH&HLYP) or the CAM-QTP family which was specifically designed to yields good ionization energies.

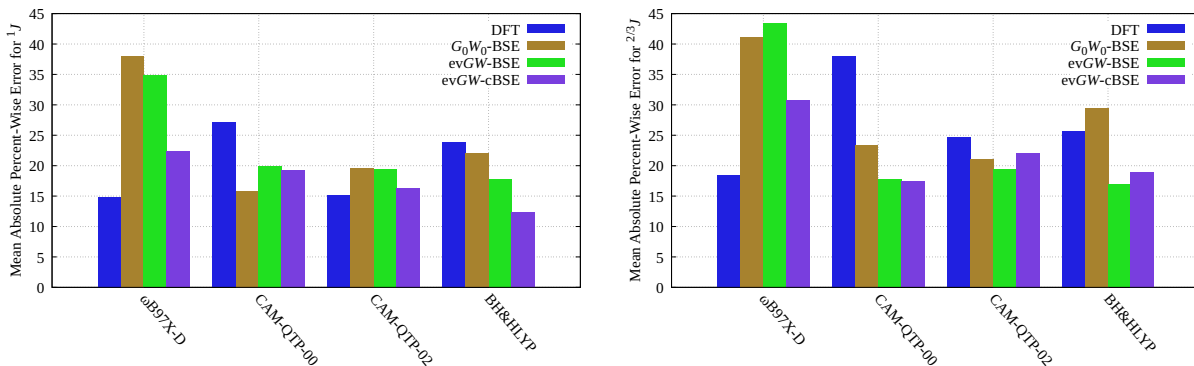


Figure 4: Mean absolute percent-wise error for NMR 1J coupling constants (left panel) and NMR $^{2/3}J$ coupling constants (right panel) with respect to the CC3/aug-ccJ-pVTZ reference values of Ref. 43. ω B97X-D is one of the top performers for Kohn–Sham DFT. Results are taken from Refs. 44 (Kohn–Sham DFT) and 37 (GW-BSE). The test set consists of 13 molecules and 45 NMR chemically inequivalent coupling constants.

The excellent performance of the evGW-cBSE based on a BH&HLYP starting point is not restricted to small systems. Notably, it can be readily applied to study the Karplus curve of tin compounds at the relativistic two-component level, which treats scalar-relativistic and spin–orbit effects on an equal footing. According to the Karplus equation, the NMR 3J coupling constant of the molecules $(\text{CH}_3)_3\text{Sn-CH}_2\text{-CHR-SnMe}_3$, with R being different substituents, follows the relation

$$^3J(\phi) = A \cos(2\phi) + B \cos(\phi) + C \quad (46)$$

where ϕ denotes the torsion angle and A, B, C are constants or fit parameters. To study this relation and the accuracy of the BSE framework for larger systems, 13 different substituents ranging from a simple hydrogen atom to the trimethylstannyl group are used and the torsion angles are varied from 0 to 180°. First, a Boltzmann-average then allows to compare the calculated coupling constants to the experimental findings⁴⁵ for each substituent as shown in the left panel of Figure 5. Here, the cBSE substantially reduces the deviation from the experiment compared to the conventional DFT approach. Secondly, an average over the 13 compounds at each angle allows to plot the coupling constants vs. the torsion angle and fit the results to Eq. 46. As indicated by a coefficient of determination of $R^2 = 0.99$, this fit to the Karplus relation works excellently. That is, cBSE successfully accounts for the triplet inaccuracies of the original BSE approach.

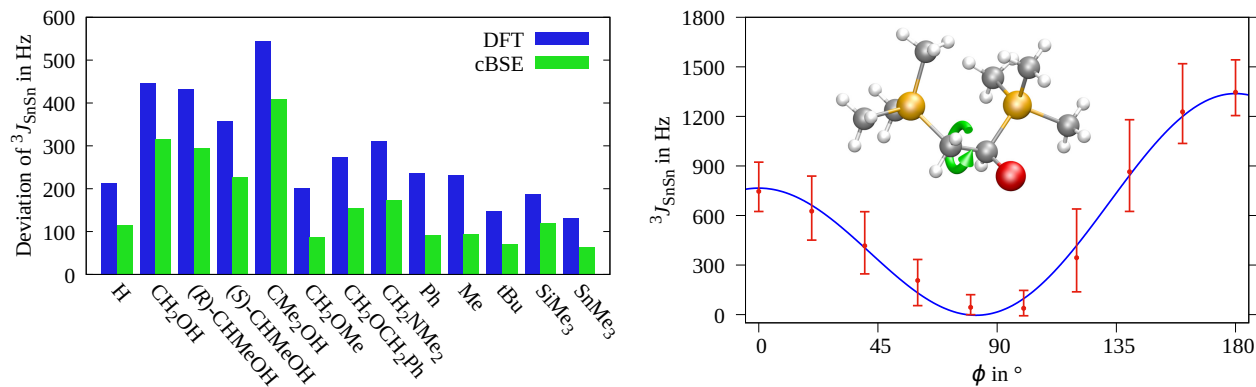


Figure 5: Left panel: Deviations of the Boltzmann-averaged coupling constants of the 13 tin compounds. Deviations with the BH&HLYP functional are shown in blue and those with evGW-cBSE@BH&HLYP in green. Abbreviations: Me = methyl, Ph = phenyl, tBu = tert-butyl, *S* = sinister, *R* = rectus. Right panel: For each tin–tin torsion angle ϕ , the average of the ${}^3J_{\text{SnSn}}$ coupling constant over the 13 compounds is given (red dot) as well as the total range spanned (vertical bars) at the evGW-cBSE@BH&HLYP/x2cTZVPall-2c level. A fitted Karplus equation is given in blue. Fit parameters for Eq. 46 are $A = 518$ Hz, $B = -286$ Hz, $C = 534$ Hz. The torsion angle and the molecular structure are illustrated above the fit. Color code: white hydrogen, gray carbon, golden tin, red substituent R. Reproduced (adapted) from Y. J. Franzke, C. Holzer, F. Mack, *J. Chem. Theory Comput.* **2022**, *18*, 1030–1045. Copyright the Authors. Published by American Chemical Society.

Taking together, the BSE can be successfully applied beyond light-matter interactions. The computational protocol for NMR coupling constants relies on evGW and a suitable functional approximation. This dependence on the Kohn–Sham starting point could be mitigated by the qsGW approach. Unfortunately, qsGW is often plagued by convergence issues and comes with increased computational costs.

Ground-State Correlation Energies and General Properties

We finally note that another important step in the direction of ground-state molecular properties was taken in Refs. 46 and 47, where the authors calculated the BSE ground-state correlation energy of small molecules with the adiabatic-connection fluctuation-dissipation theorem.⁴⁸ Bond lengths, potential energy curves, and vibrational frequencies were subsequently obtained numerically. Here, the BSE correlation energy is given by an integration over the coupling strength

parameter λ and reads^{46,48}

$$E_c = \frac{1}{2} \int_0^1 d\lambda \text{Tr}(\mathbf{C}\mathbf{D}_\lambda) \quad (47)$$

with the interaction kernel \mathbf{C} at full coupling strength ($\lambda = 1$) defined as

$$\mathbf{C} = \mathbf{C}_{\lambda=1} = \begin{pmatrix} \tilde{\mathbf{A}} & \tilde{\mathbf{B}} \\ \tilde{\mathbf{B}}^* & \tilde{\mathbf{A}}^* \end{pmatrix} \quad (48)$$

Here, the matrices $\tilde{\mathbf{A}}$ and $\tilde{\mathbf{B}}$ are a simplified form of the BSE quantities,

$$\tilde{A}_{ai,bj} = (ai|jb) \quad (49)$$

$$\tilde{B}_{ai,bj} = (ai|bj) \quad (50)$$

Eqs. 49 and 50 resemble the interaction kernel of the direct random phase approximation (RPA), which illustrates the relationship of the RPA and *GW*-BSE methods. \mathbf{D}_λ is the correlation part of the two-electron density matrix at a given coupling strength

$$\mathbf{D}_\lambda = \begin{pmatrix} \mathbf{Y}_\lambda \mathbf{Y}_\lambda^\dagger & \mathbf{Y}_\lambda \mathbf{X}_\lambda^\dagger \\ \mathbf{X}_\lambda \mathbf{Y}_\lambda^\dagger & \mathbf{X}_\lambda \mathbf{X}_\lambda^\dagger \end{pmatrix}^* - \begin{pmatrix} \mathbf{0} & \mathbf{0} \\ \mathbf{0} & \mathbf{1} \end{pmatrix} \quad (51)$$

where the vectors \mathbf{X} and \mathbf{Y} are obtained by solving the general problem described by Eq. 1 with the accordingly modified matrix elements of \mathbf{A}_λ and \mathbf{B}_λ . The subscript λ indicates that the two-electron integrals in Eqs. 2 and 3 are scaled by the coupling strength parameter λ . We stress that both \mathbf{C} and \mathbf{D}_λ are Hermitian. As usual, the equations can be simplified for closed-shell systems and real-valued orbitals as shown in Ref. 47. The total energy is calculated by adding the nuclear repulsion energy and the electronic Hartree–Fock energy to the obtained correlation energy. Formally, the correlation energy in Eq. 47 may be used to construct a Lagrangian similar to the application of the random-phase approximation to molecular properties in analytical derivative theory.⁴⁹ Unfortunately, the calculation of the BSE correlation energy is still plagued by stability

issues when the regular BSE expressions for the matrices \mathbf{A} and \mathbf{B} are applied and simply scaled with λ . This can be resolved by completely deriving the screened exchange at a given coupling strength.⁴⁶ Still, unphysical irregularities are observed for the ground-state potential energy surfaces which are due to the quasiparticle energies. In detail, these issues arise from discontinuities of the *GW* quasiparticle energies as a function of the interatomic distance or bond length.⁴⁷ This issue limits the applicability of Eq. 47 in practice and may prevent structure optimizations for both ground states and excited states.

A special case of a correlation energy obtained from the BSE is the intermolecular dispersion energy, that can be obtained from symmetry adapted perturbation theory (SAPT). It can be evaluated from the an integration over the imaginary axis of the dipole polarizability of the two molecular systems **1** and **2**,⁵⁰

$$E_c^{\text{disp.}} = \frac{1}{2\pi} \int_0^\infty d\omega \sum_{ai,bj} \gamma_{ai}^{\alpha,1}(i\omega) \gamma_{bj}^{\alpha,2}(i\omega) (ai|bj) \quad (52)$$

The quality of dispersion energies calculated from the BSE is therefore tightly linked to the quality of polarizabilities. As outlined earlier in Table 2, these can be assumed to be very high. Accordingly, Ref. 50 found high quality molecular interaction energies for van der Waals-bonded systems, clearly exceeding the quality of state-of-the-art DFT based prediction as outlined in Table 4. For the weakly bonded benzene-imidazole and benzene-pyrrole systems, both G_0W_0 -BSE and *evGW*-BSE based SAPT only deviate by a fraction of a kJ/mol from reference coupled cluster singles, doubles, and perturbative triples (CCSD(T)) values. The basis set dependence for these calculations is more pronounced than the dependence on the quasiparticle energies, as the deviation between results from G_0W_0 and *evGW* is smaller than the deviation between results from different basis sets or the correction from the explicitly correlated F12 ansatz. As CCSD(T) with large basis sets is considered the gold standard for van der Waals-bonded systems, this hints at correlation energies from the BSE being very accurate in certain cases.

Table 4: Electronic binding energy D_e (in kJ/mol) of benzene-imidazole (Bz·Im) and benzene-pyrrole (Bz·Py) calculated at the SAPT(Method)/aug-cc-pV(D/T/Q)Z level of theory. GW -BSE results calculated at the PBE0 Kohn–Sham reference. Results are taken from Ref. 50.

| Method | aug-cc-pVDZ | | aug-cc-pVTZ | | aug-cc-pVQZ | |
|---------------|-------------|-------|-------------|-------|-------------|-------|
| | Bz·Im | Bz·Py | Bz·Im | Bz·Py | Bz·Im | Bz·Py |
| PBE0AC | 24.2 | 21.5 | 23.1 | 20.8 | – | – |
| +F12 | 26.1 | 23.4 | 23.8 | 21.4 | – | – |
| G_0W_0 -BSE | 20.5 | 18.3 | 22.1 | 19.9 | 22.4 | 20.2 |
| +F12 | 22.5 | 20.2 | 22.8 | 20.5 | 22.7 | 20.5 |
| evGW-BSE | 20.1 | 17.9 | 21.5 | 19.4 | – | – |
| +F12 | 22.0 | 19.8 | 22.2 | 20.0 | – | – |
| CCSD(T) | 19.6 | 17.5 | 21.9 | 19.7 | – | – |
| +(F12)(T*) | 22.3 | 20.0 | 22.8 | 20.4 | 22.8 | 20.5 |

Summary and Possible Future Directions

This review outlines that the Bethe–Salpeter equation method has well advanced past the point of mainly being useful for simulating linear optical spectra. During the last few years, methods to also simulate various properties, including polarizabilities, hyperpolarizabilities, two-photon absorption, transient absorption, optical rotation, NMR properties, and properties linked with these have emerged. Properties evaluated from the BSE have been shown to be very reliable, often outperforming TD-DFT at the same computational scaling. For example, the general weakness of TD-DFT, frequently being unable to properly describe charge-transfer or Rydberg excitations is cured by the BSE, in turn also leading to an improved description of polarizabilities and other properties. And while TD-DFT certainly remains competitive, the ever-growing number of functionals are both a blessing and a curse—a blessing because there will likely be at least one density functional that works, and a curse because it gets evermore challenging to identify the correct one. The BSE method outlined in this review removes the challenge of finding the correct functional, replacing it with a more rigorous approach from first principles. Most of the dependence on the underlying functional is removed by the preceding GW step, and results from the combined GW -BSE approach are therefore robust. This is an incredibly valuable feature, and we therefore expect the

BSE to be a growing competition to TD-DFT on the prediction of properties over the next decade.

Finally, a current trend in calculating correlation energies from the BSE has emerged and proven useful to study the underlying physics of many-electron systems. The BSE is there used to restore the electron-electron interaction, leading to an improved description of the fluctuations taking place in this delicate process. Further, the *GW*-BSE can even be applied to a many-Fermions framework going beyond electrons within a multicomponent ansatz to compute excitation energies. When using a common Hilbert space for the RI auxiliary basis sets, the working equations for the *GW* quasiparticles can be derived in a straightforward way and used to set up the BSE Hessian matrices.⁵¹ This suggests that also response properties could become available for this framework in the near future.

Data Availability Statement

No new data were generated or analyzed in support of this study.

Author Contributions and Declarations

Christof Holzer: Conceptualization (equal); Investigation (equal); Methodology (equal); Validation (equal); Visualization (equal); Writing – original draft (equal); Writing – review & editing (equal).

Yannick J. Franzke: Conceptualization (equal); Investigation (equal); Methodology (equal); Validation (equal); Visualization (equal); Writing – original draft (equal); Writing – review & editing (equal).

Notes

The authors declare no competing financial interest.

Acknowledgement

C.H. gratefully acknowledges the Volkswagen Stiftung for financial support. Y.J.F. gratefully acknowledges support via the Walter–Benjamin programme funded by the Deutsche Forschungsgemeinschaft (DFG, German Research Foundation) — 518707327.

References

- (1) Blase, X.; Duchemin, I.; Jacquemin, D.; Loos, P.-F. The Bethe–Salpeter Equation Formalism: From Physics to Chemistry. *J. Chem. Phys. Lett.* **2020**, *11*, 7371–7382, DOI: 10.1021/acs.jpcllett.0c01875.
- (2) Casida, M. E. Time-dependent density-functional theory for molecules and molecular solids. *J. Mol. Struct.: THEOCHEM* **2009**, *914*, 3–18, DOI: 10.1016/j.theochem.2009.08.018.
- (3) Golze, D.; Dvorak, M.; Rinke, P. The *GW* compendium: A practical guide to theoretical photoemission spectroscopy. *Front. Chem.* **2019**, *7*, 377, DOI: 10.3389/fchem.2019.00377.
- (4) Gui, X.; Holzer, C.; Klopper, W. Accuracy Assessment of *GW* Starting Points for Calculating Molecular Excitation Energies Using the Bethe–Salpeter Formalism. *J. Chem. Theory Comput.* **2018**, *14*, 2127–2136, DOI: 10.1021/acs.jctc.8b00014.
- (5) Li, J.; Golze, D.; Yang, W. Combining Renormalized Singles *GW* Methods with the Bethe–Salpeter Equation for Accurate Neutral Excitation Energies. *J. Chem. Theory Comput.* **2022**, *18*, 6637–6645, DOI: 10.1021/acs.jctc.2c00686.
- (6) Blase, X.; Duchemin, I.; Jacquemin, D. The Bethe–Salpeter equation in chemistry: relations with TD-DFT, applications and challenges. *Chem. Soc. Rev.* **2018**, *47*, 1022–1043, DOI: 10.1039/C7CS00049A.
- (7) Rohlfing, M.; Louie, S. G. Excitonic Effects and the Optical Absorption Spec-

- trum of Hydrogenated Si Clusters. *Phys. Rev. Lett.* **1998**, *80*, 3320–3323, DOI: 10.1103/PhysRevLett.80.3320.
- (8) Faber, C.; Boulanger, P.; Duchemin, I.; Attaccalite, C.; Blase, X. Many-body Green’s function *GW* and Bethe–Salpeter study of the optical excitations in a paradigmatic model dipeptide. *J. Chem. Phys.* **2013**, *139*, 194308, DOI: 10.1063/1.4830236.
- (9) Holzer, C.; Klopper, W. Ionized, electron-attached, and excited states of molecular systems with spin–orbit coupling: Two-component *GW* and Bethe–Salpeter implementations. *J. Chem. Phys.* **2019**, *150*, 204116, DOI: 10.1063/1.5094244.
- (10) Bintrim, S. J.; Berkelbach, T. C. Full-frequency dynamical Bethe–Salpeter equation without frequency and a study of double excitations. *J. Chem. Phys.* **2022**, *156*, 044114, DOI: 10.1063/5.0074434.
- (11) Kaplan, F.; Harding, M. E.; Seiler, C.; Weigend, F.; Evers, F.; van Setten, M. J. Quasi-Particle Self-Consistent *GW* for Molecules. *J. Chem. Theory Comput.* **2016**, *12*, 2528–2541, DOI: 10.1021/acs.jctc.5b01238.
- (12) Holzer, C. Practical Post-Kohn–Sham Methods for Time-Reversal Symmetry Breaking References. *J. Chem. Theory Comput.* **2023**, *19*, 3131–3145, DOI: 10.1021/acs.jctc.3c00156.
- (13) Ren, X.; Rinke, P.; Blum, V.; Wieferink, J.; Tkatchenko, A.; Sanfilippo, A.; Reuter, K.; Scheffler, M. Resolution-of-identity approach to Hartree–Fock, hybrid density functionals, RPA, MP2 and *GW* with numeric atom-centered orbital basis functions. *New J. Phys.* **2012**, *14*, 053020, DOI: 10.1088/1367-2630/14/5/053020.
- (14) Rohlfing, M.; Louie, S. G. Electron-hole excitations and optical spectra from first principles. *Phys. Rev. B* **2000**, *62*, 4927–4944, DOI: 10.1103/PhysRevB.62.4927.
- (15) Leng, X.; Jin, F.; Wei, M.; Ma, Y. *GW* method and Bethe–Salpeter equation for calculating

- electronic excitations. *Wiley Interdiscip. Rev.: Comput. Mol. Sci.* **2016**, *6*, 532–550, DOI: 10.1002/wcms.1265.
- (16) Förster, A.; Visscher, L. Quasiparticle Self-Consistent *GW*-Bethe–Salpeter Equation Calculations for Large Chromophoric Systems. *J. Chem Theory Comput.* **2022**, *18*, 6779–6793, DOI: 10.1021/acs.jctc.2c00531.
- (17) Yu, V. W.-z.; Jin, Y.; Galli, G.; Govoni, M. GPU-Accelerated Solution of the Bethe–Salpeter Equation for Large and Heterogeneous Systems. *J. Chem Theory Comput.* **2024**, *20*, 10899–10911, DOI: 10.1021/acs.jctc.4c01253.
- (18) Holzer, C.; Pausch, A.; Klopper, W. The *GW*/BSE Method in Magnetic Fields. *Front. Chem.* **2021**, *9*, 746162, DOI: 10.3389/fchem.2021.746162.
- (19) Ghosh, S.; Deb, B. Dynamic polarizability of many-electron systems within a time-dependent density-functional theory. *Chem. Phys.* **1982**, *71*, 295–306, DOI: 10.1016/0301-0104(82)87030-4.
- (20) Jamorski, C.; Casida, M. E.; Salahub, D. R. Dynamic polarizabilities and excitation spectra from a molecular implementation of time-dependent density-functional response theory: N₂ as a case study. *J. Chem. Phys.* **1996**, *104*, 5134–5147, DOI: 10.1063/1.471140.
- (21) Kehry, M.; Franzke, Y. J.; Holzer, C.; Klopper, W. Quasirelativistic two-component core excitations and polarisabilities from a damped-response formulation of the Bethe–Salpeter equation. *Mol. Phys.* **2020**, *118*, e1755064, DOI: 10.1080/00268976.2020.1755064.
- (22) Kehry, M.; Klopper, W.; Holzer, C. Robust relativistic many-body Green’s function based approaches for assessing core ionized and excited states. *J. Chem. Phys.* **2023**, *159*, 044116, DOI: 10.1063/5.0160265.
- (23) Goebel, D.; Hohm, U. Comparative study of the dipole polarizability of the metallocenes

- Fe(C₅H₅)₂, Ru(C₅H₅)₂ and Os(C₅H₅)₂. *J. Chem. Soc., Faraday Trans.* **1997**, *93*, 3467–3472, DOI: 10.1039/A702715J.
- (24) Rocca, D.; Lu, D.; Galli, G. Ab initio calculations of optical absorption spectra: Solution of the Bethe–Salpeter equation within density matrix perturbation theory. *J. Chem. Phys.* **2010**, *133*, 164109, DOI: 10.1063/1.3494540.
- (25) Parker, S. M.; Rappoport, D.; Furche, F. Quadratic Response Properties from TDDFT: Trials and Tribulations. *J. Chem. Theory Comput.* **2018**, *14*, 807–819, DOI: 10.1021/acs.jctc.7b01008.
- (26) Rauwolf, N.; Klopper, W.; Holzer, C. Non-linear light–matter interactions from the Bethe–Salpeter equation. *J. Chem. Phys.* **2024**, *160*, 061101, DOI: 10.1063/5.0191499.
- (27) Villalobos-Castro, J.; Knysh, I.; Jacquemin, D.; Duchemin, I.; Blase, X. Lagrangian Z-vector approach to Bethe–Salpeter analytic gradients: Assessing approximations. *J. Chem. Phys.* **2023**, *159*, 024116, DOI: 10.1063/5.0156687.
- (28) Himmelsbach, P.; Holzer, C. Excited state properties from the Bethe–Salpeter equation: State-to-state transitions and spin–orbit coupling. *J. Chem. Phys.* **2024**, *161*, 244105, DOI: 10.1063/5.0244254.
- (29) Kaatz, P.; Donley, E. A.; Shelton, D. P. A comparison of molecular hyperpolarizabilities from gas and liquid phase measurements. *J. Chem. Phys.* **1998**, *108*, 849–856, DOI: 10.1063/1.475448.
- (30) Couling, V. W.; Shelton, D. P. Hyperpolarizability dispersion measured for (CH₃)₂O. *J. Chem. Phys.* **2015**, *143*, 224307, DOI: 10.1063/1.4936865.
- (31) Bauernschmitt, R.; Ahlrichs, R. Stability analysis for solutions of the closed shell Kohn–Sham equation. *J. Chem. Phys.* **1996**, *104*, 9047–9052, DOI: 10.1063/1.471637.

- (32) Knysh, I.; Villalobos-Castro, J. D. J.; Duchemin, I.; Blase, X.; Jacquemin, D. Excess and excited-state dipole moments of real-life dyes: a comparison between wave-function, BSE/GW, and TD-DFT values. *Phys. Chem. Chem. Phys.* **2023**, *25*, 29993–30004, DOI: 10.1039/D3CP04467J.
- (33) Knysh, I.; Villalobos-Castro, J. D. J.; Duchemin, I.; Blase, X.; Jacquemin, D. Exploring Bethe–Salpeter Excited-State Dipoles: The Challenging Case of Increasingly Long Push–Pull Oligomers. *J. Phys. Chem. Lett.* **2023**, *14*, 3727–3734, DOI: 10.1021/acs.jpcllett.3c00699.
- (34) Çaylak, O.; Baumeier, B. Excited-State Geometry Optimization of Small Molecules with Many-Body Green’s Functions Theory. *J. Chem Theory Comput.* **2021**, *17*, 879–888, DOI: 10.1021/acs.jctc.0c01099.
- (35) Ismail-Beigi, S.; Louie, S. G. Excited-State Forces within a First-Principles Green’s Function Formalism. *Phys. Rev. Lett.* **2003**, *90*, 076401, DOI: 10.1103/PhysRevLett.90.076401.
- (36) Helgaker, T.; Jaszuński, M.; Ruud, K. Ab initio methods for the calculation of NMR shielding and indirect spin-spin coupling constants. *Chem Rev.* **1999**, *99*, 293–352, DOI: 10.1021/cr960017t.
- (37) Franzke, Y. J.; Holzer, C.; Mack, F. NMR Coupling Constants Based on the Bethe–Salpeter Equation in the *GW* Approximation. *J. Chem. Theory Comput.* **2022**, *18*, 1030–1045, DOI: 10.1021/acs.jctc.1c00999.
- (38) Franzke, Y. J. Reducing Exact Two-Component Theory for NMR Couplings to a One-Component Approach: Efficiency and Accuracy. *J. Chem. Theory Comput.* **2023**, *19*, 2010–2028, DOI: 10.1021/acs.jctc.2c01248.
- (39) Franzke, Y. J.; Mack, F.; Weigend, F. NMR Indirect Spin–Spin Coupling Constants in a Modern Quasirelativistic Density Functional Framework. *J. Chem. Theory Comput.* **2021**, *17*, 3974–3994, DOI: 10.1021/acs.jctc.1c00167.

- (40) Jacquemin, D.; Duchemin, I.; Blondel, A.; Blase, X. Benchmark of Bethe-Salpeter for Triplet Excited-States. *J. Chem. Theory Comput.* **2017**, *13*, 767–783, DOI: 10.1021/acs.jctc.6b01169.
- (41) Rangel, T.; Hamed, S. M.; Bruneval, F.; Neaton, J. B. An assessment of low-lying excitation energies and triplet instabilities of organic molecules with an ab initio Bethe-Salpeter equation approach and the Tamm-Dancoff approximation. *J. Chem. Phys.* **2017**, *146*, 194108, DOI: 10.1063/1.4983126.
- (42) Holzer, C.; Klopper, W. Communication: A hybrid Bethe–Salpeter/time-dependent density-functional-theory approach for excitation energies. *J. Chem- Phys.* **2018**, *149*, 101101, DOI: 10.1063/1.5051028.
- (43) Faber, R.; Sauer, S. P. A.; Gauss, J. Importance of Triples Contributions to NMR Spin–Spin Coupling Constants Computed at the CC3 and CCSDT Levels. *J. Chem. Theory Comput.* **2017**, *13*, 696–709, DOI: 10.1021/acs.jctc.6b01003.
- (44) Holzer, C.; Franzke, Y. J.; Kehry, M. Assessing the Accuracy of Local Hybrid Density Functional Approximations for Molecular Response Properties. *J. Chem. Theory Comput.* **2021**, *17*, 2928–2947, DOI: 10.1021/acs.jctc.1c00203.
- (45) Mitchell, T. N.; Kowall, B. Karplus-type dihedral angle dependence for the coupling constants $^3J(^{119}\text{Sn}-\text{C}-\text{C}-^{119}\text{Sn})$ and $^3J(^{119}\text{Sn}-\text{C}-\text{C}-^{29}\text{Si})$. *Magn. Reson. Chem.* **1995**, *33*, 325–328, DOI: 10.1002/mrc.1260330502.
- (46) Holzer, C.; Gui, X.; Harding, M. E.; Kresse, G.; Helgaker, T.; Klopper, W. Bethe–Salpeter correlation energies of atoms and molecules. *J. Chem. Phys.* **2018**, *149*, 144106, DOI: 10.1063/1.5047030.
- (47) Loos, P.-F.; Scemama, A.; Duchemin, I.; Jacquemin, D.; Blase, X. Pros and Cons of the Bethe–Salpeter Formalism for Ground-State Energies. *J. Phys. Chem. Lett.* **2020**, *11*, 3536–3545, DOI: 10.1021/acs.jpcllett.0c00460.

- (48) Maggio, E.; Kresse, G. Correlation energy for the homogeneous electron gas: Exact Bethe-Salpeter solution and an approximate evaluation. *Phys. Rev. B* **2016**, *93*, 235113, DOI: 10.1103/PhysRevB.93.235113.
- (49) Rekkedal, J.; Coriani, S.; Iozzi, M. F.; Teale, A. M.; Helgaker, T.; Pedersen, T. B. Communication: Analytic gradients in the random-phase approximation. *J. Chem. Phys.* **2013**, *139*, 081101, DOI: 10.1063/1.4819399.
- (50) Holzer, C.; Klopper, W. Communication: Symmetry-adapted perturbation theory with intermolecular induction and dispersion energies from the Bethe–Salpeter equation. *J. Chem. Phys.* **2017**, *147*, 181101, DOI: 10.1063/1.5007929.
- (51) Holzer, C.; Franzke, Y. J. Beyond Electrons: Correlation and Self-Energy in Multi-component Density Functional Theory. *ChemPhysChem* **2024**, *25*, e202400120, DOI: 10.1002/cphc.202400120.